Diffraction-limited observations of astronomical sources with a rotation shearing interferometer in the near infrared

Ghez P.[1], Mariotti J.-M.[2], Monin J.-L.[1], Perrier C.[3], Dainty C.[4] and Fuensalida J.J.[5]

(1) Observatoire de Grenoble, CERMO, BP 53X, 38041 Grenoble Cedex, France.
(2) Observatoire de Paris-Meudon, DESPA, France.
(3) Observatoire de Lyon, 69561 St-Genis-Laval, France.
(4) Imperial College, London, United Kingdom.
(5) Instituto de Astrofisica de Canarias, La Laguna, Tenerife, Spain.

ABSTRACT

We present an experiment aimed at diffraction-limited imaging of astronomical sources in the 2-5 μm range. It is based on a rotation shearing interferometer that produces fringes in the pupil plane that can be scanned through the zero optical path difference. The two-dimensional interferograms are recorded with an infrared camera looking at the recombined pupil image. The modulus and the phase of the Fourier transform of the object intensity distribution are derived from these interferograms. The main advantage of this technique is its constant transfer function that makes it independent of seeing variations and instrumental aberrations.

We describe the experiment set-up and discuss some simulation results which illustrate the operation of the interferometer. We present astronomical data recently obtained at the 4.20m William Herschel Telescope of the Royal Greenwich Observatory in La Palma, and results on the circumstellar shell star NML Cygni.

1. INTRODUCTION

Infrared astronomy has made fast and impressive progress in the last two decades due to the development of infrared mono-detectors and, more recently, detectors arrays. It now spans a considerable part of modern astrophysics and covers a lot of astrophysical fields that were even not recognized before the advent of performant infrared detectors. Near infrared, i.e. from 1 to 5 microns, is, in particular, the wavelength window where thermal emission by cold matter, such as warm dust, or the coldest stars takes place. Therefore this range is specially well suited for tackling all questions related to properties of faint low mass stars, to mass-loss by red giant and supergiant stars, to the dynamics of dust accretion leading to star formation and to the strong emission by active galactic nuclei.

But most of these phenomena actually show up at very small angular scale with respect to the resolution that telescopes can achieve at infrared wavelengths. Characteristic scales are below a few arcsecs and, for a vast majority of the closest objects of interest, below one arcsec or a value even smaller if statistical studies are desirable. Moreover, phenomena such as those with a complex dynamics are likely to hide their fundamental properties in intricate structures that insufficient resolution would blur strongly enough to prevent us from ever unveiling them.

The resolution of ground-based infrared observations, just as visible ones, is limited by image blurring by the turbulent atmosphere. Astronomers now tend to select excellent sites in terms of image quality but even so the images are always spread over a "seeing" disc of about one arcsec. To overcome this limitation astronomers have developped interferometric techniques that aim at extracting diffraction-limited images from turbulence-blurred images. At two microns for instance, a 4m-class telescope provides a diffraction-limited resolution of 0.12 arcsec after complete image recovery.

Several techniques have been developped on the largest telescopes to reach this limit. We describe here a prototype version of an infrared shearing interferometer that has been previously

tested[1] at Haute Provence Observatory and recently installed at the GHRIL (Ground-based High Resolution Imaging Laboratory) focus of the William Herschel Telescope (WHT) at La Palma.

2. METHOD

Until now most results from high resolution imaging have been obtained with speckle techniques that are based on series of short exposures recorded in the focal plane. Although quite easy to implement, these techniques have a serious drawback due to the high dependence of the average transfer function on the seeing variations. Estimation of the complex visibility giving the object spectrum is thus made extremely difficult; this is specially true for the modulus which requires a careful calibration against a point-like source. The seeing variations make this procedure usually both time-consuming and not free of artefacts.

It is why we have chosen to apply to the infrared domain the rotation shearing interferometric technique, already successfully tested in the visible by Roddier and Roddier[2,3]. It extracts the visibility directly from pupil plane observations. In practice the beam from the telescope is splitted into halves inside an interferometer, one of the beams is rotated around its axis and the two are then interfered. The fringe pattern thus created in the image of the telescope pupil yields a measure of the source complex degree of coherence γ that is also the source complex visibility. The transfer function is constant over the frequency domain covered or, in other words, independent of phase variations due to atmospheric pathlength fluctuations or due to instrumental aberrations. This property makes the technique essentially self-calibrated i.e. relaxes the need for transfer function calibration. It also yields, as an additional advantage, a high single image signal-to-noise ratio (SNR) on bright sources whereas the SNR saturates at unity for speckle techniques. As a result, unlike speckle practice, it is possible to obtain a definite result with a few exposures on a bright source and to reach unprecedented dynamical ranges in diffraction-limited imaging.

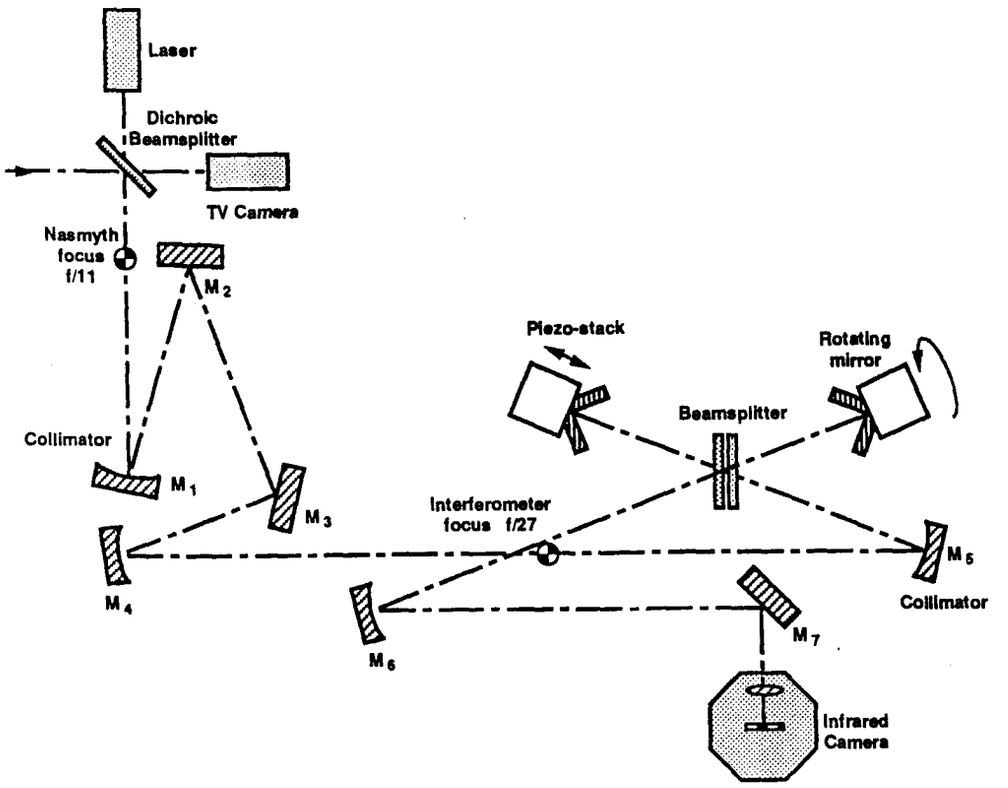

Fig. 1. Optical scheme of the rotation shearing interferometer

The actual implementation of our prototype is based on a Michelson's interferometer that provides the pupil rotation with roof mirrors installed on both arms, one of them being rotatable in order to control the shear angle. In practice, we mostly use a 180 degrees shear which gives access to the full spatial frequency coverage up to the diffraction limit of the telescope. The optical scheme (Fig. 1) is essentially the same that the one described in Mariotti *et al* [1] except for the additional mirrors (M1 to M4) needed to adapt the focal ratio of the WHT (f/11) to the one of the interferometer (f/27). The detector is an infrared array (IRCCD) on which the image of the recombined pupil is formed.

From shearing interferograms the degree of coherence of the wavefront can be extracted from spatial analysis based on the local contrast of the fringes[2,3]. This technique requires a large number of pixels and is well suited for the visible domain where photon noise dominates. In the near infrared range however, the observations should be detector noise limited, which requires as small as possible a number of pixels be used to extract the information: this is why we have chosen the Phase Shifting Interferometry (PSI) approach. In this technique the fringes are fluffed-out, hence minimizing the number of pixels, and their contrast and phase is extracted via temporal modulation of the optical path difference (OPD) of the interferometer: the second roof-mirror is mounted on a piezo-stack which scans the OPD through four positions with quarter-wavelength increments (Fig. 2). For each position an infrared image is recorded and the process is repeated after each set of four frames. In order to correctly freeze the seeing, the four frames have to be recorded in a total time smaller than the coherence time of the atmospherical turbulence.

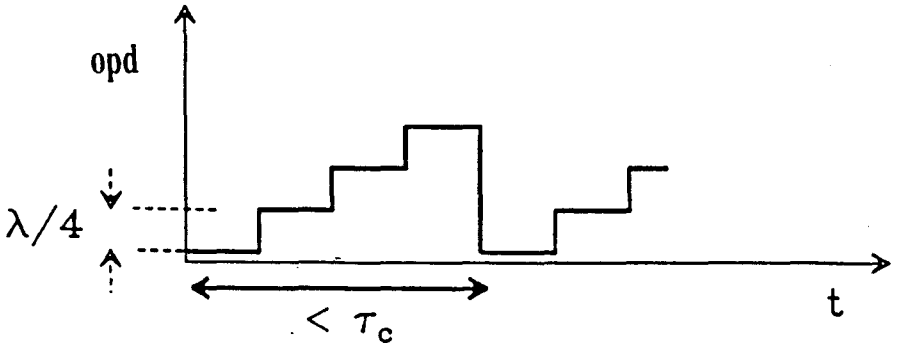

Fig. 2. Modulation of the optical path difference

3. DATA REDUCTION AND MODELISATION

3.1 Estimation of the visibility function

As a first approximation, let us assume that our detector has a linear flux response defined by the quantum efficiency η and a fixed pattern plus dark current C only functions of the integration time. If B is the background flux and if the noise is neglected, the two-dimensional interferograms are expressed for one given pixel by:

$$I_i = C + \eta B + \eta P[1 + |\gamma| \cos(\phi + \phi_a + (i-1)\frac{\pi}{2})] \qquad (1)$$

where i runs over the steps of the piezo-stack, P is the flux from the star (referred to as "photometry" in the following), ϕ is the phase of γ the complex degree of coherence ($\gamma = |\gamma| e^{i\phi}$) and ϕ_a is the phase introduced by the atmospheric turbulence. The photometric term can be extracted from Eq. (1):

$$P_s = \frac{1}{4} \sum_{i=1,4} I_{s_i} = C + \eta B + \eta P \qquad (2)$$

where the index s indicates a measure on the source. Combining this with a measure on the sky background:

$$P_b = C + \eta B,$$

we deduce the photometric term for the source:

$$\eta P = P_s - P_b$$

The interference terms are computed from the four frames. Let X be the *cosine* term and Y the *sine* one:

$$X = \frac{1}{2}(I_1 - I_3) = \eta P|\gamma|\cos(\phi + \phi_a) \qquad (3)$$

and

$$Y = \frac{1}{2}(I_4 - I_2) = \eta P|\gamma|\sin(\phi + \phi_a) \qquad (4)$$

Let now A be the amplitude of the fringes :

$$A^2 = X^2 + Y^2 = \eta^2 P^2 |\gamma|^2,$$

we can compute the square of the 2-D visibility V of the source :

$$V^2 = \frac{A^2}{(P_s - P_b)^2} = |\gamma|^2 \qquad (5)$$

If the atmospheric turbulence is well frozen over the four frames, the disturbed phase ϕ_a does not change and it cancels out when computing the amplitude or the photometry. So, the amplitude term is not affected by turbulence and we can average it over the images recorded. This leads to the final squared visibility:

$$< V^2 >= < \frac{A^2}{(P_s - P_b)^2} > \qquad (6)$$

which shows that the experiment is self-calibrated.

3.2 Modelisation

3.2.1 Parameters

We checked our reduction algorithm by using numerical models of interferograms and applying the procedure to them. The models include the following parameters:

- the constants of the experiment: B, P, η and γ.

- the noise, as produced by various sources: firstly, each frame is affected by a noise σ_f in order to simulate the read-out noise (at 2.2 μm) or the photon noise of the thermal background (at higher wavelengths). Also, we introduce a phase noise σ_ϕ i.e. either noise on the position of the piezo driven mirror or a phase shift induced by the fact that the atmosphere is not perfectly frozen between steps of the piezo-stack. Finally, we add scintillation noise i.e. a variation of the photometric term.

- a simple model of atmospheric turbulence which produces maps of phase errors ϕ_a.

The modeled interferograms take the form, for a given pixel and image j and step i of the piezo:

$$I_{ji} = \eta B + \sigma_{f_{ji}} + \eta P_j[1 + |\gamma|\cos(\phi_{a_j} + \sigma_{\phi_i} + (i-1)\frac{\pi}{2})]$$

3.2.2 Test of the reduction procedure with the model

The essential limitations of the experiment come from sampling problems and are the following:
The wavefront tilt introduced by guiding errors and turbulence yields an air wedge in the interferometer whence a spatial modulation of the fringes. We must correctly sample these fringes i.e. have at least 2 pixels per fringe. If the pupil of the telescope is imaged on $N \times N$ pixels, we cannot have more than $N/2$ fringes in the interferogram. In practice $N \sim 16$.
The main effect of turbulence is to destroy the spatial correlation of the phase. To estimate correctly the fringe contrast, we need to sample the coherence cells with at least two by two pixels.
The third condition is to freeze the atmospheric turbulence within the four steps of the OPD modulation.

The main results of the tests performed with this model were to show that the reduction procedure was correct, and to emphasize the effects of undersampling. For average seeing conditions they dominate the degradation of the estimation of the contrast: to avoid this problem and to reach the theoretical SNR, it is necessary to select only the well-sampled images. For typical conditions, only about one third of the images are retained.

3.3 Data reduction

The visibility function of the object obtained by Eq. (6) is likely affected by instrumental effects, especially optical ones. For a given set-up, to get rid of these effects, one must calibrate the Transfer Function with the visibility obtained on an unresolved source. Similarly to other interferometric techniques, this calibrated visibility can be used to extract relevant parameters on the source by means of model fitting.

Moreover, estimation of the complex visibility leads to the possibility of image reconstruction, which implies knowledge of the phase ϕ. This is not yet available in our data reduction procedure but, as a first step, we can derive the autocorrelation function of the reconstructed image from the squared visibility.

A specific problem of pupil-plane interferometry lies in the central obstruction of the telescope primary mirror which hides the low frequencies of the visibility[3]. For this preliminary work, we have solved the problem by merely extrapolating the visibility inwards down to the zero frequency.

4. RESULTS

4.1 Optical Simulations

For testing purpose, we set up the experiment at Lyon Observatory and performed optical simulations. The source was a halogene lamp with a pin-hole located at a focus of the experiment. This allowed us to assess the performances of the optics, electronics and acquisition procedure under favorable conditions, i.e. without atmospheric turbulence and with a very bright source. Applying the whole reduction process led to the visibility (Fig. 3) and autocorrelation function of the image of the pin-hole (Fig. 4). At 3.8 μm the source is fully resolved by the interferometer.

Because these data were not affected by turbulence, we had a straight-forward access to the complex visibility function, and therefore to the reconstructed image of the test object (Fig. 5).

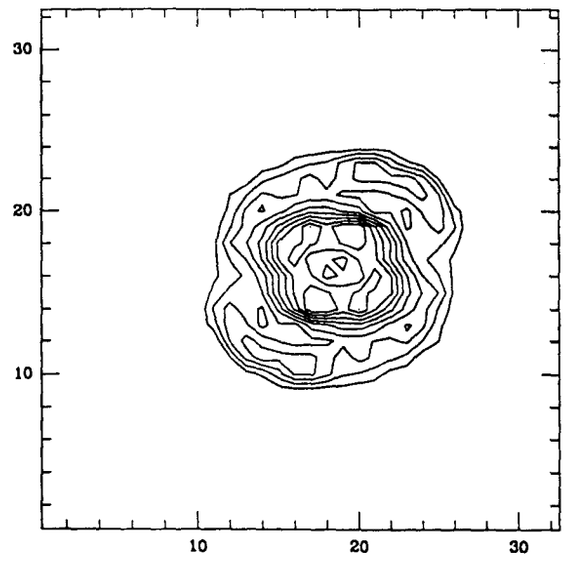

Fig. 3. Visibility function of the test source (arbitrary units)

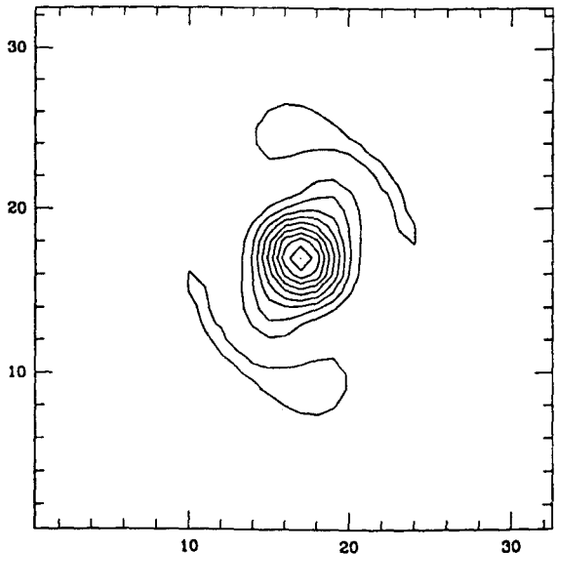

Fig. 4. Autocorrelation function of the test source (arbitrary units)

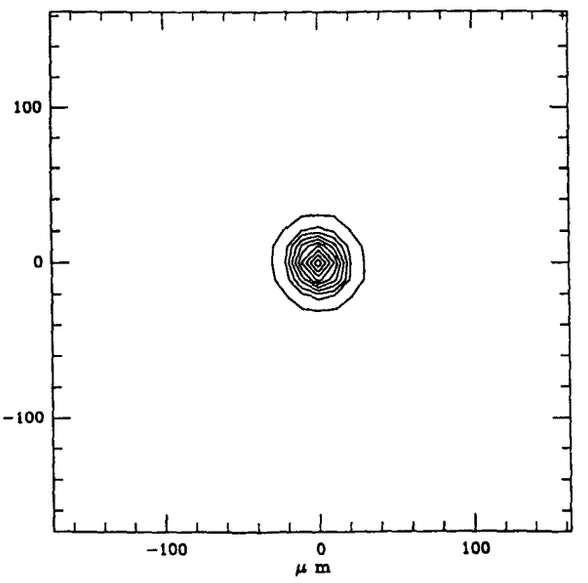

Fig. 5. Image reconstruction of the test source

4.2 First results on astronomical sources

We have performed observations at the 4.20m WHT of the Royal Greenwich Observatory located in La Palma (Canary Islands). On the night of April 13 (1990) we could record good quality data at the wavelength of 3.8 μm on two objects: NML Cygni, a star known to be surrounded by a circumstellar shell[4,5,6], and α1 Herculi, an M5 supergiant unresolved by a 4.2 meter telescope at this wavelength.

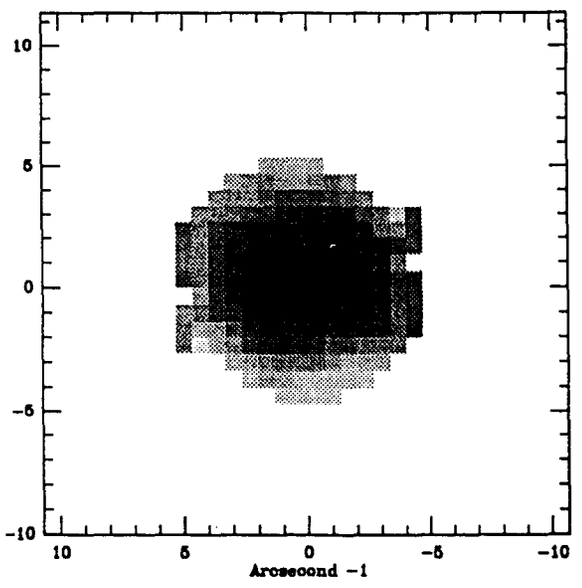

Fig. 6. Visibility function of NML Cygni calibrated by α1 Herculi

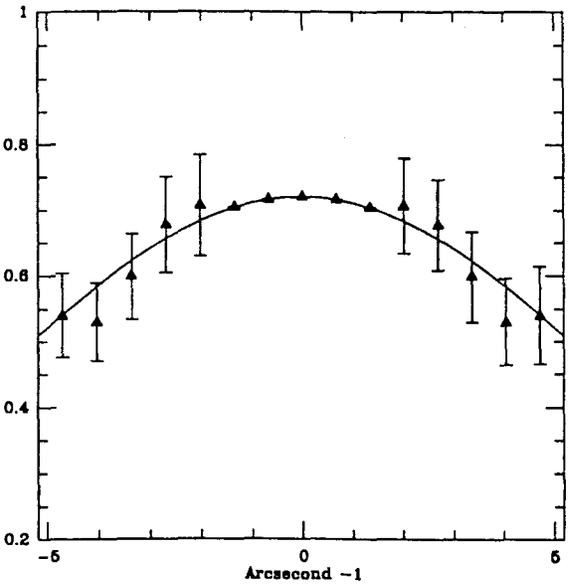

Fig. 7. Section in the visibility of NML Cygni

The visibility function of NML Cyg, calibrated by the visibility function of the unresolved reference α1 Her, shows as expected a depression at high frequency indicating that the source is marginally resolved (Fig. 6 and Fig. 7). The visibility decreases from $\sim$0.7 at 2 arcsec^{-1} to $\sim$0.5 at 5 arcsec^{-1}. These values are in good agreement with previously published visibility curves for this source[4,5,6]. It can be noted also a clear departure from central symmetry. Assuming a gaussian shape, we can derive 1/e widths for the long and short axis of symmetry, respectively 9.8 and 6.2 arcsec^{-1}, with a relative incertitude of $\sim$ 10%. They correspond in the image plane to full widths at half-maximum (FWHM) of 0.05 and 0.09 arcsec respectively. However, these values should be taken with caution, as the gaussian model does not fit well the central part of the visibility. By forcing the visibility to 1 at the zero frequency, we obtain new FWHMs of 0.09 and 0.12 arcsec, in better agreement with the result obtained by Dyck *et al* [5], but at the expense of a degradation in the quality of the fit: clearly, the structure of NML Cyg departs from a mere gaussian shape. We also note that McCarthy[4] reported an asymmetry of this source at 5 μm which compares very well with our values.

Finally, the figures 8 and 9 illustrate the autocorrelation function of the reconstructed image of NML Cyg.

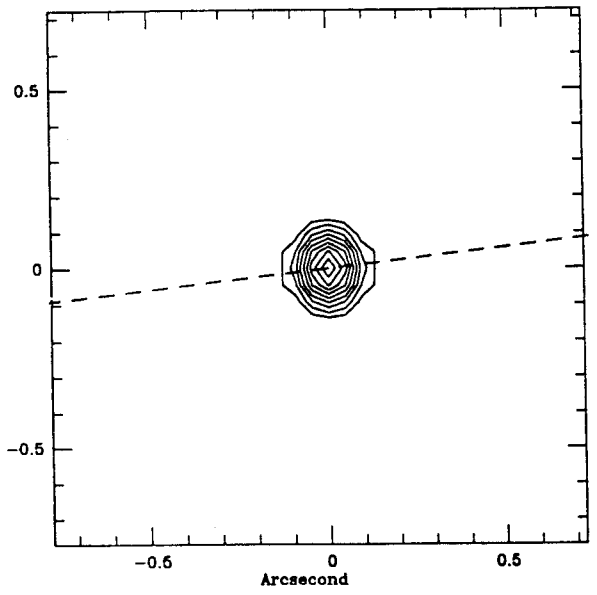

Fig. 8. Autocorrelation function of NML Cygni calibrated by α1 Herculi

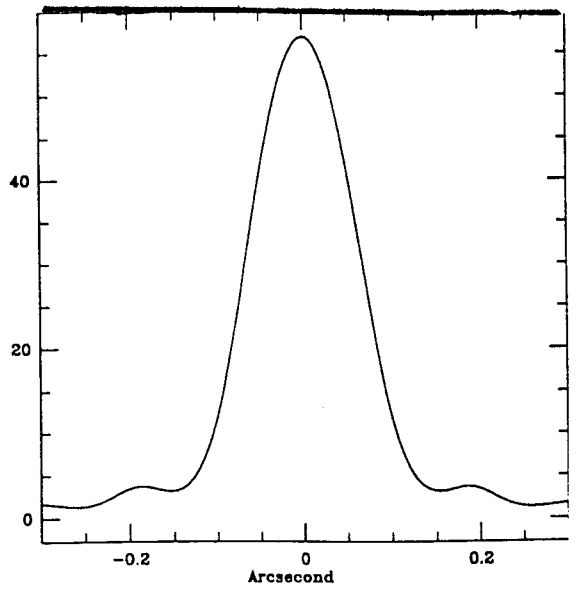

Fig. 9. Section in the autocorrelation function of NML Cygni and PSF

5. CONCLUSION

We have presented in this paper the first diffraction-limited observations at infrared wavelengths with a rotation shearing interferometer on a large telescope. The preliminary results emphasize the advantage of pupil analysis in term of Signal to Noise Ratio on the visibility, especially at the high frequencies, yielding a good dynamical range image from a very limited series of short exposures.

The next step will involve an extensive study of the encountered limitations or possible biases, and the restoration of the visibility phase. The progress already observed with our present set-up and still limited reduction algorithms makes us confident that astrophysical exploitation of rotation shearing interferometry in the near infrared is within reach.

ACKNOWLEDGMENTS

The set-up of the interferometer at the GHRIL laboratory of the WHT and the observations would not have been possible without the help of the GHRIL manager Mike Breare. Many thanks also to Andrew Zadrozny and Panayoti Petmezakis. The experiment has been funded by the Institut National des Sciences de l'Univers, which also financed the shipment of the equipment and the travels of the french observers to La Palma.

The William Herschel Telescope is operated on the island of La Palma by the Royal Greenwich Observatory in the Spanish Observatorio del Roque de los Muchachos of the Instituto de Astrofisica de Canarias.

REFERENCES

1. Mariotti, J.-M., Monin, J.-L., Zadrozny, A. and Perrier, C., 1988, in proc. of NOAO/ESO Conference on *High Resolution Imaging by Interferometry*, ed. F. Merkle, Garching, March 1988.

2. Roddier, C. and Roddier, F. 1979, in proc. of IAU Coll. No. 49, p. 175.

3. Roddier, C. and Roddier, F. 1989, in *Diffraction limited imaging with very large telescopes*, NATO ASI Vol. C 274, ed. D. Alloin and J.-M. Mariotti, Cargèse, September 1988.

4. McCarthy, D.W., 1979, in proc. IAU Coll. No. 50, *High Angular Resolution Stellar Interferometry*, ed. J. Davis and W.J. Tango, p. 18-1.

5. Dyck, H.M., Zuckerman, B., Leinert, C. and Beckwith, S., 1984, Ap. J. **287**, 810–813.

6. Christou, J. and Ridgway, S.T., 1989, B.A.A.S. **21**, 1112.